April 2025

The CFD Potentiality on the AUV Hydrodynamic Design

Diego VILLA [a,1], and Stefano GAGGERO [a]
[a] *Univeristy of Genova, Genova, Italy.*
ORCiD ID: Diego VILLA https://orcid.org/0000-0001-6332-705X, Stefano GAGGERO https://orcid.org/0000-0001-8470-2955

Abstract. Hydrodynamic aspects of autonomous underwater vehicles, even if often underestimated, play a crucial role in the overall vessel design. Over the past few decades, computational fluid dynamics has become a widely used tool for investigating complex hydrodynamic problems in a fast and reliable way, often substituting the most expensive and time-consuming experimental campaigns. Nevertheless, even if several researchers adopt these approaches to investigate some specific aspect (i.e. vehicle resistance, PMM tests, etc.), from an industrial point of view they are rarely used in the vehicle design stages (in particular during the preliminary ones), because of vehicles designs are primary driven by control aspects (i.e. payload arrangements, propulsion layout, etc.). The present paper tries to show possible research fields where these numerical tools can provide a valuable contribution to their design. Different aspects are investigated, ranging from the typical ones, such as the impact of the vehicle geometry on the resistance, to the most complex ones, such as hull-propeller interactions in hovering conditions. This activity demonstrates that a more deep knowledge of these hydrodynamic aspects can better drive the vehicle design, obtaining a more effective and efficient design.

Keywords. RANS code, AUV design, Manoeuvrability

1. Introduction

Autonomous Underwater Vehicles (AUVs) have gained importance in recent decades thanks to their capability to explore marine areas autonomously for research, environmental control, safety, and security reasons. This technology is a valuable instrument for improving boundary control in coastal countries ([1]). Even if their diffusion growed over time, their design is still demanded to satisfy mainly control aspects (such as the ability to follow a prescribed path autonomously), often disregarding relevant hydrodynamic aspects of the vehicle. This is rooted in historical and engineering factors, such as the fact that these vehicles should have strong control capability in complex scenarios, making the control aspects predominant with respect to the others. The last decades research fields, in fact, is focused on control aspects as, for instance, in [2] where a new AUV was designed for seabed pipeline survey or in [3] where the underwater mine marine exploration was the primary AUV design purposes, or in [4] where the logic for

[1]Corresponding Author: Diego Villa, contact details.

the coordinated navigation of several AUVs were explored. Nevertheless, to realistically assess control strategies, it is necessary to define the hydrodynamic forces developed by the AUV because, with respect to other autonomous vehicles (i.e ground or air ones), the interactions with the surrounding fluid are of primary importance to reliably define its motion [5]. Generally, these types of simulators are based on lumped coefficient models [6], where the quantification of the model coefficients (named hydrodynamic coefficients) can be achieved through experimental tests (EFD) (see [9]), analytical or semi-empirical methods (ASE) or computational fluid dynamics (CFD) [8,7,10,11]. Regarding the CFD-based models, often the focus is on specific aspects as the vehicle resistance, or the identification of the maneuvering coefficients or the optimization of the geometries. This paper, differently, tries to demonstrate the overall capability and the potential benefits of the systematic application of modern CFD techniques (in the present case, an open-source viscous flow code) to the hydrodynamic design of AUVs.

The paper is organized as follows: after a brief description of the geometry considered (section 2), an overview of the numerical tool adopted is reported (section 3), and then some applications are investigated to demonstrate the potentiality of the CFD codes (section 4). Finally, some conclusions are reported.

2. Reference geometry

As reference geometry, a realistic counter-mine vehicle has been considered. Figure 1 shows the selected shape with the focus on the propulsion layout. The vehicle is 3x1.25x0.6m in length, beam and height, respectively. It is equipped with two ducted propellers (red surfaces) located in the stern part for normal navigation, able to push the vessel at the design speed of about 3m/s. The maneuvering abilities have been guaranteed by four later thrusters (white tunnels) positioned, two at the bow and two at the middle stern part of the vehicle, with an inclination, with respect to the horizontal plane, of $\pm 45°$. This configuration has been selected for its known effectiveness from a control point of view. Two vertical rudders (violet surfaces) are located in the slipstream of the two main navigation propellers for vertical fly control. For stability reasons, indeed, horizontal and vertical fixed surfaces (green in the figure) have been located in the stern part of the vessel.

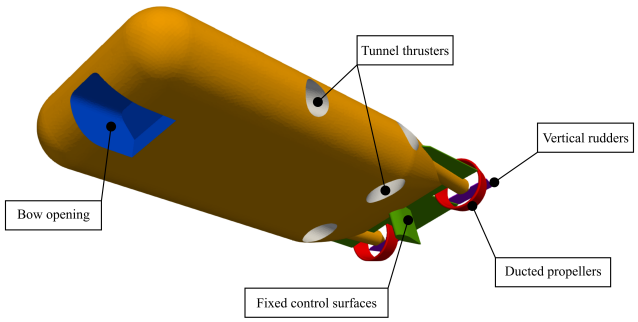

Figure 1. 3-D sketch of the reference AUV geometry.

3. Numerical methodology

The numerical code adopted is the open-source CFD code *OpenFOAM v.8*. It adopts the finite-volume approach to discretize the flow governing equations. The average single-phase incompressible equations following the approach proposed by Reynolds have been accounted for representing the effect of the turbulence (i.e. the RANS approach). The steady-state regime is considered to speed up the analyses, also in light of the quite significant number of calculations needed. This simplification neglects the unsteadiness generated by the body, in particular when it assumes a non-streamlined position with respect to the main flow direction, but it drastically reduces the overall computational time. Considering that the average forces are of interest during the first design stages, this assumption can be considered well-posed. The hydrodynamic aspects connected with the propulsion system are fundamental, particularly when complex motions are considered (i.e. the hovering condition). Different approaches can be adopted to include the propeller in a viscous calculation, ranging from the fully resolved approach to the body-force one. The former discretize the exact geometry of the propulsion system into the code, solving all the flow quantities related to the propeller. This approach, even if it could be considered the most accurate one, requires a special mesh treatment to account for the relative motion between the blades and the vehicle, making the computation intrinsically unsteady. To overcome this aspect, often a Moving Reference Frame (MRF) approach can be adopted. It discretises the blade geometries within the vehicle itself. However, it considers the propeller region as a separate region where the flow equations are solved with respect to a rotating reference frame. This approach overcomes the mesh motion issues and the consequent unsteadiness, being the new equations steady in its reference frame, but it requires significant computational resources due to the grid density needed around the propeller blades. In addition, if the propeller is subject to a non-symmetrical inflow field, the solution depends on the considered blade position. The more straightforward and most used approach when an average value is of interest is, differently, the body-force one. It consists of the inclusion of only the time averaged propeller effect on the vehicle flow field. This can be obtained by imposing a body force field into the propeller region without the need to include its geometry. This approach is the least computationally demanding, and at the same time, the propeller forces can be obtained by separate tools (like ones based on potential flow or estimated by the inflow condition itself). For the present calculations, also considering the aim of the work, this latest approach has been preferred.

All the computations have been carried out using a box domain with an extension of 6x3x3 (LxBxD) times the vehicle length, respectively (see Figure 2). These sizes

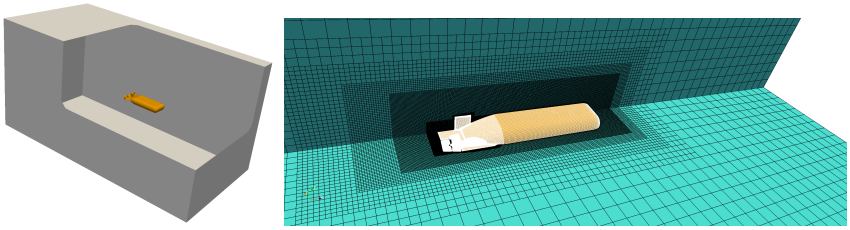

Figure 2. Domain view (left) and example of the mesh arrangement (right).

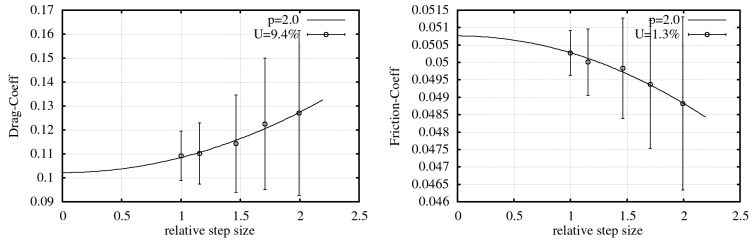

Figure 3. Uncertainty Assessment (UA) for the total drag and the friction part.

have been considered as an optimal compromise between the computational time and the resultant accuracy. The mesh is generated by a hex-dominant cartesian mesher with local refinements in the near-field of the vehicle. The refinements have been appropriately designed to guarantee a homogeneous density in the wake field regardless of the flow direction with respect to the vehicle. A mesh of about 2 million cells has been considered as the reference for the simpler geometry (bare-hull at forward speed), and it increases up to 4 million when more geometrical details are included (such as the propeller tunnels). A mesh dependence analysis has been performed for the bare-hull configuration at forward speed using six mesh sizes from 1.5 up to 12 million cells and following the procedure proposed in [12]. As shown in Figure 3, an uncertainty less than 10% has been obtained for the global forces (the drag) and lower than 1.5% for the friction part. Even if a quite significant Uncertainty Assessment (UA) is reported, it can be considered acceptable for the activity aim.

4. Results

The possibilities provided by the CFD codes to deeply investigate the flow dynamic around moving objects can be utilized for different aims, such as the analyses of the impact of the geometries details, the evaluation of the most efficient running attitude or the creation of a physical based simulator. In the following subsections, some examples of the results obtained for the reference geometry will be reported.

4.1. Impact of the vehicle geometry on the resistance

One of the most impacting aspects of the ship design is correlated with the evaluation of the vehicle resistance. Considering that these AUVs mainly operate in deep water conditions, their resistance may be split into friction and pressure components. Suppose that the first component can be easily estimated using friction lines, as the one proposed by the ITTC in the Recommended Procedures and Guidelines. In that case, the pressure part is almost constant regardless of the flow speed (if no turbulent/laminar transition occurs). For the reference geometry in fully appended configuration, the non-dimensional resistance is substantially constant, and only the friction part varied with the Reynolds number, as expected. Moreover, from the figure 4, it is evident that the pressure part is twice the friction one, fostering the importance of the use of CFD tools.

Often, for operation constraints, these type of vehicles requires the presence of some recess on the hull to accommodate some particular instruments. In the reference geome-

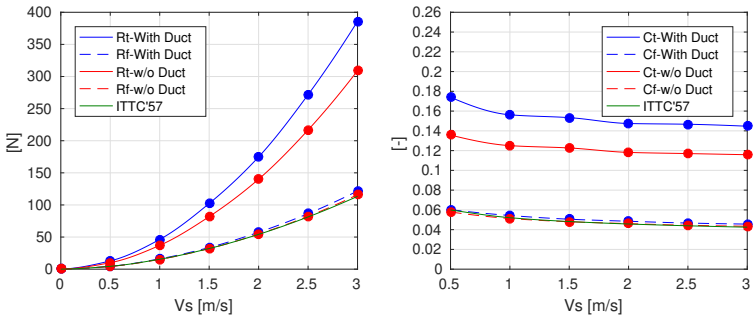

Figure 4. Resistance prediction with (red) and without (blue) ducts, in dimensional (left) and non-dimensional (right) form.

try, an opening in the bow part has been analysed (i.e. used for articulated arms or other interacting devices). Even if an impact on the resistance can be expected, the CFD calculations quantify this effect (see Figure 5 top), showing that the resistance increment is more than 100% of the overall longitudinal force. It is interesting to note that only 45% of this additional drag is directly due to the pressure peak on the inner frontal area and 20% to the presence of the transverse tunnels. Still, the other part is due to an increment of the main body force. This can be explained by Figure 5 in the two bottom figures, where a wide re-circulation zone is generated in the lower part of the vehicle, destroying the pressure recovery at the stern.

Even if the CFD codes are generally powerful tools, their results should be considered carefully. An example is the analysis of the presence of the tunnel thrusters and their impact on the vehicle's resistance. When a symmetrical object is tested, no lateral forces are expected, but some asymmetry can be generated due to the presence of significant transversal holes.

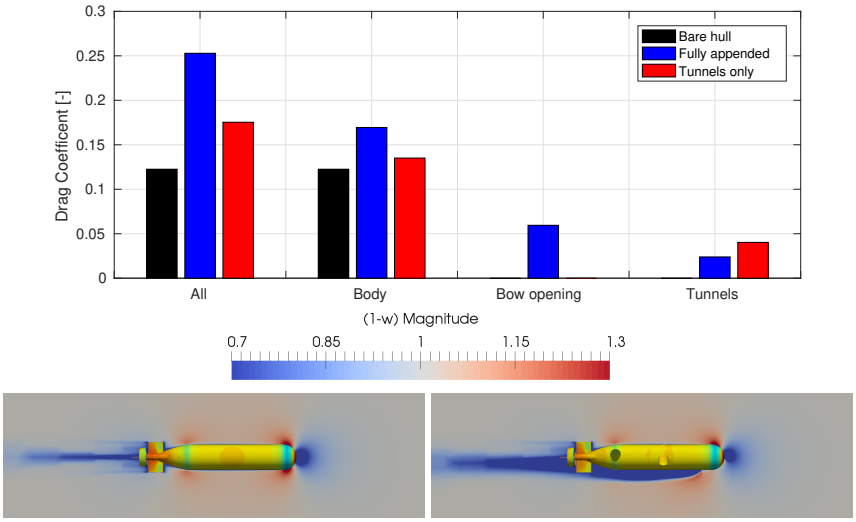

Figure 5. Comparison of the non-dimensional drag between different geometries.

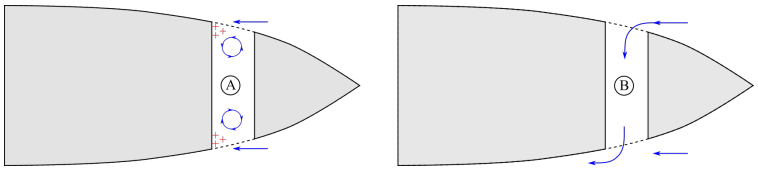

Figure 6. Comparison of the nondimensional drag between different bow geometries.

Figure 6 depicts the possible configurations assumed by a flow field in correspondence with transversal holes. In the configuration named (a), a symmetrical behavior is maintained, generating a quite strong pressure field in the cavities, which have a consequence on the resistance. Despite this, if some asymmetries arise, the flow can start to pass through the hole, completely changing the flow behavior; see configuration (b). The presence of an outflow from one side of the cavity generates an additional local drag. Both conditions can be considered feasible. During towing tank tests, this (well-known) effect is reduced by introducing a dummy propeller in the cavity to reproduce the real presence of the propulsion system, which generally counteracts the creation of the configuration (b) for the most experienced configuration (a). If the tunnel thrusters are quite small, they have a minor impact on the resistance for ships; differently, if they are big, as in the present case, their impact on the overall performance could be significant. Some numerical tests have been performed to highlight this effect, considering open and closed tunnels or with a dummy propeller. The reported results (Figure 7) show that, when the tunnels are open, and the configuration (b) take place, an increment of the resistance of more than 100% can be recorded. Differently, if the configuration (a) is maintained (closing the or adding the dummy propeller) less than 20% of drag increment is recorded. For the sake of completeness, considering that the dummy propeller better reproduces the real condition for the other analyses, this geometry is considered as the reference one.

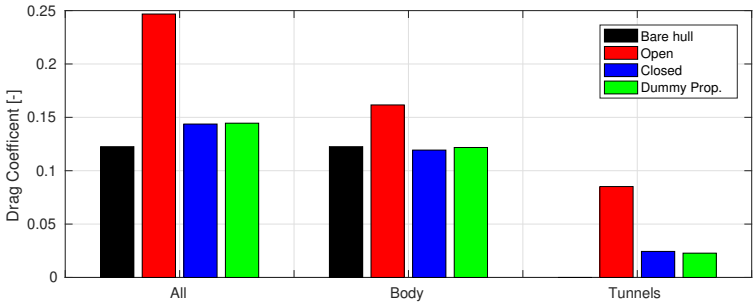

Figure 7. Comparison of the nondimensional drag between different tunnels treatment.

4.2. Self-propulsion analyses

One of the main aims for which the resistance is required is to design the correct propulsion system to reach the requested design speed. In this contest, there are two main aspects: the inflow velocity field seen by the propeller and the requested thrust. The numerical procedure, widely adopted in the marine field (see among the others [13,14,15]), summarized these aspects using two nondimensional parameters: the wake fraction (w)

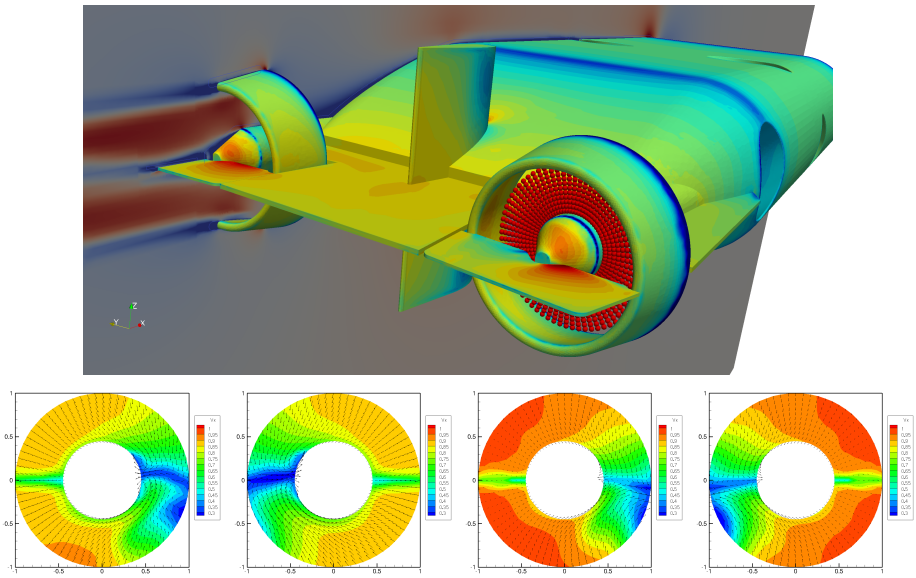

Figure 8. Top: extraction points of the propeller wakes. Bottom: Wakes without duct (left) and with duct (right).

and the thrust deduction factor (t). The former represents the average velocity of the propeller with respect to the vehicle speed; the latter expresses the requested thrust with respect to the towing resistance. These analyses have been performed using the body force approach, including the average effect generated by the propeller, which provides the thrust in equilibrium with the drag.

The virtual towing tank tests can easily extract the wake fraction as the velocity field in the propeller disk. Figures 8 show the two wakes for the propulsion system, considering or not the presence of the duct. In both fields, the hull wake and the presence of the horizontal fins are well captured (velocity reductions at 90 and 270 degrees), as is the acceleration induced by the presence of the duct (extended red areas). Differently, the thrust deduction factor can be extracted using the simulations with the body forces as the vehicle drag increases. Table 1 reports the comparison between the thrust deduction factors, including or excluding the presence of the duct. Even if the factor is more severe for the configuration without duct, the total thrust is indeed lower because the reference ship drag is lower. This analysis is a clear example of how the CFD can help the AUV designer properly design the propulsion system.

One of the main drawbacks of this analysis is connected with the often unrealistic condition intrinsically considered in these calculations. In fact, an AUV is never neutral (weight equal to buoyancy) under the water, so to keep the quote constant, some actions should be done. Two strategies could be adopted: use the vertical thruster with a consequently energy consumption or fly with a prescribed trim able to counteract the vertical unbalance of forces. The prediction of this condition can be estimated by using the CFD by means of a series of calculations where the angle of trim and the horizontal rudder deflection are systematically varied to explore how the hydrodynamic vertical force and yaw moment are. Figure 9 depicts their behavior versus the deflection angle at different vehicle pitches, showing almost linear trends, as expected due to the small angles in-

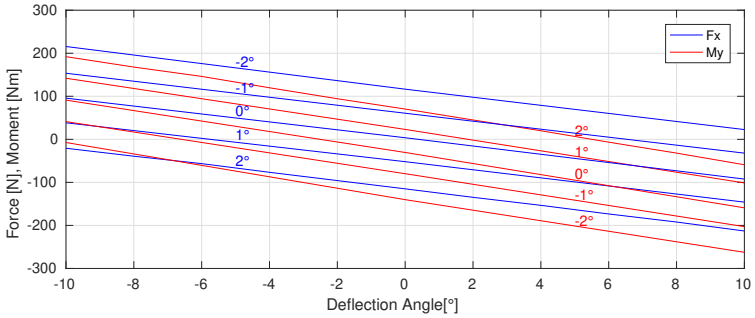

Figure 9. Top: extraction points of the propeller wakes. Bottom: Wakes without duct (left) and with duct (right).

volved. Then, by solving the two linear equations representing the equilibrium condition, the most efficient condition can be easily obtained.

4.3. Maneuvering

The main focus of an AUV design isn't generally on the propulsion aspects. Still, considering that it operates most of the time in maneuvering conditions (such as hovering conditions), more attention is devoted to the maneuverability aspects. For this reason, the ability to correctly predict the hydrodynamic forces experienced by the vehicle with different flow directions is a fundamental task. The CFD codes can also help the designer with these aspects. Typically, the simulations are devoted to assessing the vehicle forces and moments when different flow directions are considered (this configuration reproduces a body moving with a generic speed in calm water, or equivalently a fixed object into a sea current). These calculations require a significant number of tests to explore the overall possible configurations because the possible directions are represented by two free parameters: the drift angle (β from 0° to 180° for symmetry) and the elevation (γ from -90° to 90°). As an example, to effectively explore the space, as shown in figure 10 on the left, more than 70 simulations have been used to assess the forces and moments behavior. Some peculiar aspects arise from the calculations, such as the wing effect. When the flow comes from the top or the bottom (Z direction), due to the bow-stern asymmetry, a significant longitudinal force is predicted (10 times stronger than the vehicle resistance). Figure 10 on the right shows the non-dimensional forces and moments varying the elevation. The wing effect is well visible for angles around 90° and -90°, where a positive longitudinal force is depicted. For the sake of completeness, its

Table 1. Non dimensional self-propulsion coefficients with and without duct.

	No Duct				With Duct			
Speed [m/s]	Rt [N]	T[N]	(1-w)	(1-t)	Rt [N]	T[N]	(1-w)	(1-t)
0.5	12.9	13.53	0.711	0.953	10.06	11.64	0.789	0.864
1	46.31	50.23	0.731	0.922	37.07	43.86	0.805	0.845
1.5	102.29	108.98	0.724	0.939	81.82	93.8	0.814	0.872
2	174.8	189.52	0.73	0.922	140.11	161.49	0.804	0.868
2.5	271.72	291.34	0.742	0.933	216.74	249.23	0.813	0.87
3	385.95	414.09	0.754	0.932	309.01	352.66	0.828	0.876

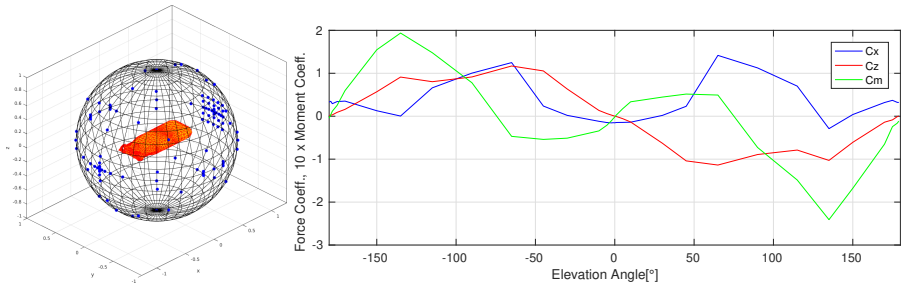

Figure 10. Example of the flow direction considered (right) and the non-dimensional forces and moments variing the elevation angle (left)

dimensional value is, however, less than 20% of the corresponding vertical force. These findings can be considered additional proof of the importance of using the CFD in the AUV design.

Another application where the CFD tools can provide a deeper insight is related to the interaction effect of the maneuvering propulsors (lateral thrusters) on the hull forces. Generally, the maneuvering simulators take into account the hull forces (the ones previously mentioned) and the active propellers as isolated devices with only some weak interactions by means of some coefficients (for instance, the thrust deduction factors). For AUVs, differently, these interactions could be significant, and the numerical tools can provide an insight into it. As an example, a first analysis is here reported, where the pure crabbing conditions (i.e. $\beta = 90^{\circ}$) generated by its own actuators is investigated. An allocation matrix can be easily obtained by knowing the propulsors' geometrical layout. This matrix provides the thrust needed for each device to generate the prescribed forces and moments. An iterative process has been developed to assess the equilibrium. Firstly, knowing the hull forces in pure crabbing condition, the actuators have been set to the requested thrust (using the allocation matrix), imposing the equilibrium. Then, the simulation was run, including the propeller effects of each actuator as body forces. This simulation, due to the presence of the slipstream flow generated by the propellers, evaluates a new set of hull forces. Consequently, the previously expected equilibrium is not achieved. Finally, the thrusts are updated until an equilibrium is reached. Figure 11 shows the iteration history of the actuated thrusts for each device. This equilibrium is achieved by also applying a relaxation factor to guarantee the stability of the procedure. Two main considerations arise. First, it is evident that the initial guess is not in equilibrium and during the iterations, a convergence trend is obtained even if a significant noise can be seen despite it being partially filtered out by the selected relaxation factor.

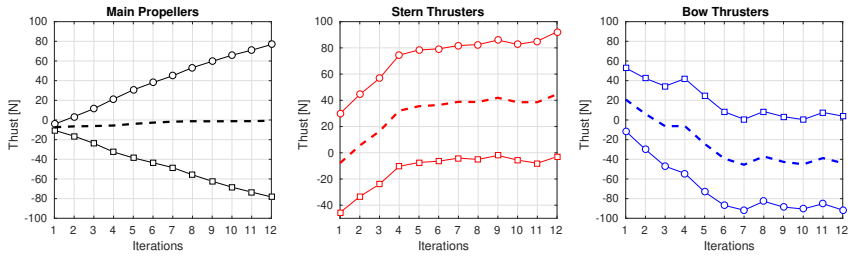

Figure 11. Convergence of the forces of each actuator (circle for rithy and square for the left side).

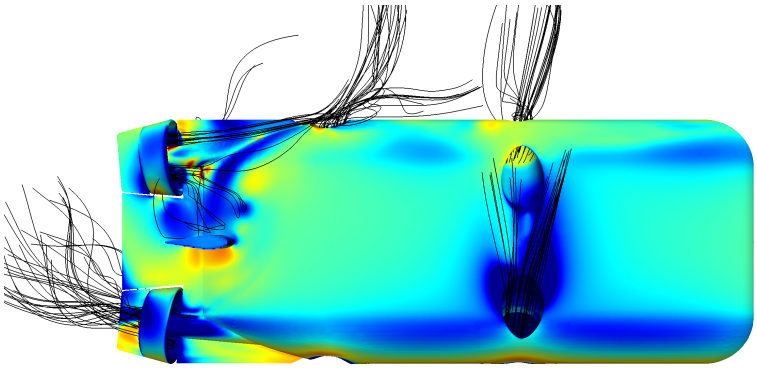

Figure 12. 3-D view of the flows generated by the actuators during a crabbing manoeuvre.

Regarding the actuators, the two lateral thrusts tend to a fixed value. Indeed, the main propellers never reach a stable condition: they show divergent behaviors. This is due to a peculiar aspect connected with the selected layout. Considering the device arrangement, the yaw moment (generated by the hull bow/stern asymmetry) can be compensated only by the two aft propellers, not directly by the transversal thrusters; otherwise, a roll moment will be induced. For this reason, the two propellers operate in opposite directions. Unfortunately, the slip stream of the reversed one interacted with the hull, generating a strong pressure field on it, which increased the yaw moment itself (see figure 12). This mechanism tends to self-amplify, generating the mentioned divergence of the equilibrium condition. Consequently, this consideration demonstrates that the selected layout should be improved to counteract the hydrodynamic forces in this type of maneuver.

5. Conclusions

This paper provides a comprehensive analysis of the hydrodynamic aspects connected with the AUV design. A reference counter-mine geometry has been selected as an example of the potentiality coming from the application of modern CFD tools. Several aspects have been highlighted from both qualitative and quantitative perspectives, ranging from the typical analyses often performed for ships, like the power predictions (resistance and self-propulsion simulations), up to the most customized analyses connected with the operability of the AUV in complex scenarios. Several food for thought arise in the activity, such as the considerations connected with the impact of geometrical aspects which, even if, the direction is often quite obviously, their quantification can help the designer to select the best compromise between efficiency and operability. Several aspects connected with the navigation efficiency have been explored easily using these tools, such as the most efficient way to counteract the buoyancy effect or the selection of the best propulsion devices. Finally, complex hydrodynamic interactions between the maneuvering actuators and the hull have been evidenced, demonstrating that their interactions are complex, generating unexpected behaviours. In conclusion, this paper widely demonstrates that modern CFD tools can provide reliable and accurate information that can improve the physical knowledge of the hydrodynamic phenomenon experienced by the AUV, making them valuable instruments for design purposes.

References

[1] Bogue, R. (2015). Underwater robots: a review of technologies and applications. Industrial Robot: An International Journal, 42(3), 186-191.

[2] Palomer, A., Ridao, P., and Ribas, D. (2019). Inspection of an underwater structure using point-cloud SLAM with an AUV and a laser scanner. Journal of field robotics, 36(8), 1333-1344.

[3] R. A. S. Fernandez, E. A. Parra R., Z. Milosevic, S. Dominguez and C. Rossi, "Design, Modeling and Control of a Spherical Autonomous Underwater Vehicle for Mine Exploration," 2018 IEEE/RSJ International Conference on Intelligent Robots and Systems (IROS), Madrid, Spain, 2018, pp. 1513-1519, doi: 10.1109/IROS.2018.8594016.

[4] Vasilijević, A., Nad, D., Mandić, F., Mišković, N., and Vukić, Z. (2017). Coordinated navigation of surface and underwater marine robotic vehicles for ocean sampling and environmental monitoring. IEEE/ASME transactions on mechatronics, 22(3), 1174-1184.

[5] Hong, L., Wang, X., and Zhang, D. S. (2024). CFD-based hydrodynamic performance investigation of autonomous underwater vehicles: A survey. Ocean Engineering, 305, 117911.

[6] Fossen, T.I., 1999. Guidance and Control of Ocean Vehicles. (Doctors Thesis). University of Trondheim, Norway, Printed by John Wiley and Sons, Chichester, England.

[7] De Barros, E. A., Pascoal, A., and De Sa, E. (2004). AUV dynamics: Modelling and parameter estimation using analytical, semi-empirical, and CFD methods. IFAC Proceedings Volumes, 37(10), 369-376.

[8] De Barros, E. A., Dantas, J. L., Pascoal, A. M., and de Sá, E. (2008). Investigation of normal force and moment coefficients for an AUV at nonlinear angle of attack and sideslip range. IEEE Journal of Oceanic Engineering, 33(4), 538-549.

[9] Roddy, R. F. (1990). Investigation of the stability and control characteristics of several configurations of the DARPA SUBOFF model (DTRC Model 5470) from captive-model experiments. David Taylor Research Center, Ship Hydromechanics Department, DTRC/SHD-1298-08.

[10] Rasekh, M., and Mahdi, M. (2022). Combining CFD, ASE, and HEKF approaches to derive all of the hydrodynamic coefficients of an axisymmetric AUV. Proceedings of the Institution of Mechanical Engineers, Part M: Journal of Engineering for the Maritime Environment, 236(2), 474-492.

[11] Zheku, V. V., Villa, D., Piaggio, B., Gaggero, S., and Viviani, M. (2023). Assessment of Numerical Captive Model Tests for Underwater Vehicles: The DARPA SUB-OFF Test Case. Journal of Marine Science and Engineering, 11(12), 2325.

[12] Eça, L., and Hoekstra, M. (2014). A procedure for the estimation of the numerical uncertainty of CFD calculations based on grid refinement studies. Journal of computational physics, 262, 104-130.

[13] Villa, D., Tani, G., Gaggero, S., Ferrando, M., Ausonio, P., Travi, P., and Viviani, M. (2023). A comprehensive analysis of a numerical self-propulsion procedure for high-speed marine vehicles. Ocean Engineering, 287, 115766.

[14] De Luca, F., Mancini, S., Pensa, C., and Raiola, G. (2018). Numerical assessment of self-propulsion factors for a fast displacement hull using different theoretical approaches. Trans R Inst Naval Arch Part B: Int J Small Craft Technol, 160, B79-B90.

[15] Wang, Z. Z., Min, S. S., Peng, F., and Shen, X. R. (2021). Comparison of self-propulsion performance between vessels with single-screw propulsion and hybrid contra-rotating podded propulsion. Ocean Engineering, 232, 109095.